# A Performance-Enhanced Antenna for Microwave Biomedical Applications by Using Metasurfaces

Danilo Brizi, *Member, IEEE*, Maria Conte, and Agostino Monorchio, *Fellow, IEEE*

***Abstract*— In this article, we introduce a novel antenna employing specifically designed metasurfaces to improve the radiating performance in close proximity to the human body, as required in microwave biomedical applications. We first present design guidelines to realize a thin metasurface acting as an impedance matching layer between the radiating element and the biological tissue, based on the transmission line equivalent model. Additionally, for the first time to the best of our knowledge, we combine an artificial magnetic conductor (AMC) as the backing element of the antenna, to improve the gain and reduce the undesired back radiation. To validate the proposed approach, we conceived a numerical test-case consisting of a bow-tie antenna operating close to a biological phantom at 2.56 GHz. Numerical simulations demonstrated the performance enhancement in terms of higher field penetration within tissues and better radiating behavior when the bow-tie antenna is working in the presence of both the metasurfaces. Furthermore, measurements carried out over fabricated prototypes confirmed the numerical results, validating the overall design procedure. The herein presented methodology can be helpful in several applications when the radiating elements operate in close proximity to biological tissues, as in medical imaging, on-body communication, mobile phones, and consumer devices.**

***Index Terms*— Biomedical applications, impedance matching, metamaterials, metasurfaces, microwave imaging.**

## I. Introduction

In THE last few decades, an ever increasing interest has been directed toward electromagnetic devices to be used in close proximity to the human body [1], [2], [3]. Consumer devices, as smartphones, smartwatches, sensors, and wearable devices, have become extremely popular, and their diffusion is expected to dramatically increase with the next generation of Internet of Things (IoT) applications within the next years [4], [5], [6], [7], [8]. Moreover, medical imaging has also recently achieved a significant evolution, pushing microwave and magnetic resonance imaging to unprecedented technological levels [9], [10], [11], [12], [13], [14], [15], [16]. Furthermore, wireless power transfer for biomedical implants is becoming the most popular technique to power stimulators and other medical devices [17], [18], [19], [20], [21], [22], [23].

All these different applications share a common ground, which is the presence of radiating elements operating in close proximity with the human body. As a matter of fact, human body strongly affects the antennas performance, since it produces detuning and impedance mismatching. Therefore, the presence of tissues degrades the antenna performance, thus limiting the effectiveness of the aforementioned applications [24], [25], [26].

For these reasons, a huge effort in the literature has been directed to address this specific aspect, and several technological solutions have been suggested so far. In particular, it has been demonstrated that interposing appropriate media (solid or liquids) between the antenna and the tissue can alleviate the mismatching issues [27]. Nevertheless, such solutions are generally cumbersome and they cannot be easily applied, especially for wearable and medical devices [28]. Indeed, very often, several layers of media are required to mitigate the impedance mismatch at the air–tissue interface [27]. To overcome such limitation, metamaterials and metasurfaces have also been proposed to relieve the tissue effects on the radiating elements. Especially, metasurfaces have received a significant research interest, due to their minimal thickness that made them easily integrable within any existing applications [29], [30], [31], [32], [33], [34]. Different works have shown how metasurfaces can act as impedance matching layers, pushing the development of technical solutions in various applications, as microwave imaging, wireless power transfer, and consumer devices [8], [35], [36], [37], [38], [39].

Nevertheless, there is a substantial lack in the literature of design guidelines of suitable metasurfaces for impedance matching purposes and radiating performance enhancement. Therefore, the potential use of metasurfaces is significantly under exploited and only moderate advantages have been proved in different works [12], [40].

To fill this gap, in this article, we present how a proper design of metasurfaces allows us to enhance the antenna radiating performance for biomedical applications. In particular, we start from an antenna design traditionally employed in several biomedical applications, i.e., the bow-tie. Then, by deriving specific and practical design guidelines based on the transmission line model, we propose the simultaneous combination of two different metasurfaces to be integrated within a single antenna. Since biological tissues placed in close proximity to a radiating device cause a significant degradation

Manuscript received 1 February 2022; revised 31 December 2022; accepted 18 January 2023. Date of publication 9 February 2023; date of current version 7 April 2023. *(Corresponding author: Danilo Brizi.)*

Danilo Brizi and Agostino Monorchio are with the Department of Information Engineering, University of Pisa, 56122 Pisa, Italy, and also with Consorzio Nazionale Interuniversitario per le Telecomunicazioni (CNIT), 43124 Parma, Italy (e-mail: danilo.brizi@unipi.it; agostino.monorchio@unipi.it).

Maria Conte is with Free Space SRL, 56127 Pisa, Italy (e-mail: maria.conte@free-space.it).

Color versions of one or more figures in this article are available at https://doi.org/10.1109/TAP.2023.3242414.

Digital Object Identifier 10.1109/TAP.2023.3242414

of its performance, a first metalayer is meant to be interposed between the bow-tie antenna and the tissue with the aim of realizing an impedance matching layer. In addition, an artificial magnetic conductor (AMC) is further introduced as a backing plane, whose purposes are: 1) reducing the undesired back radiation; 2) increasing the antenna gain; and, noticeably, 3) obtaining an overall thin structure. To the best of our knowledge, this is the first attempt to combine, at the same time, different metasurfaces to realize performance enhancement of antennas operating in close proximity to the human body. In addition, this approach can be helpful to guide the design process of effective and efficient radiating elements, avoiding cumbersome solid or liquid matching media. Finally, the huge number of full-wave simulations generally required to optimize metasurfaces' design can also be reduced.

The rest of this article is organized as follows. Section II is devoted to present the design guidelines to realize metasurfaces acting as impedance matching sheets to be interposed between the antenna and the biological tissue. Moreover, the design of AMCs to simultaneously enhance the radiating performance of the antenna is also described. Section III, instead, presents the numerical results obtained for the chosen test-case, based on a bow-tie antenna as a radiating element. In Section IV, the fabricated prototypes are described, and experimental measurements are reported. Finally, conclusion follows.

## II. Methods

In this section, we provide design guidelines to conceive metasurfaces as impedance matching layers and AMCs for simultaneously eliminating the back radiation and increasing the antenna gain for biomedical applications.

### A. Metasurfaces Design for Impedance Matching

As a matter of fact, it has been demonstrated that the transmission line model can be a very valuable tool to represent and describe the physical interactions between a traveling plane wave impinging upon a certain homogeneous medium [41]. In a first approximation, we can represent a portion of the human body placed in the close proximity of an antenna [see Fig. 1(a)] as a homogenous medium having the average properties of the considered anatomical region. If the tissue is several wavelengths thick, then the infinite thickness hypothesis can be used and the transmission line can be considered terminated on this equivalent load. Therefore, at this point, it is possible to evaluate the overall input impedance from the antenna position toward the tissue [i.e., including an eventual air gap $d_{\text{air}}$, Fig. 1(b)]. With reference to Fig. 1(b), the overall impedance $Z_{\text{input}}$ can be expressed as

$$Z_{input} = Z_0 \frac{Z_L + jZ_0 \tan(\beta d)}{Z_0 + jZ_L \tan(\beta d)}, \tag{1}$$

where $Z_0$ is the free-space characteristic impedance (377 Ω), the propagation constant in the vacuum is equal to $\beta = \omega\sqrt{\varepsilon_0\mu_0}$, whereas the biological load impedance $Z_L$ is

$$Z_L = \sqrt{\frac{\mu_0}{\varepsilon_0\varepsilon_r\left(1 - \frac{j\sigma}{\omega\varepsilon_0}\right)}}. \tag{2}$$

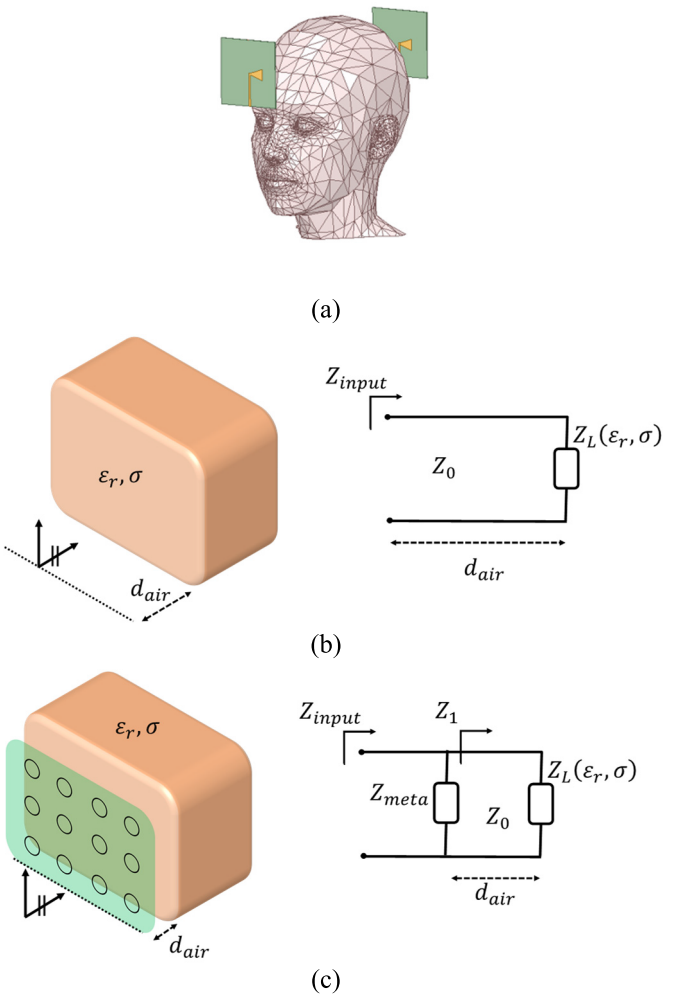


Fig. 1. (a) Pictorial representation of the proposed concept: two antennas are placed in the close proximity of a human district. (b) Schematic draw depicting a plane wave impinging upon a biological sample (left) and the equivalent transmission line model (right). (c) Same schematic depicting a plane wave impinging upon a biological sample covered with a metasurface (left) and the equivalent transmission line model (right).

The impedance behavior of the resulting equivalent model, i.e., capacitive or inductive, is an important information, even if retrieved in the simplified scenario of an impinging plane wave. Indeed, this information can be nevertheless used for the metasurface design. In particular, the metasurface can be realized in order to show an impedance behavior opposite to the tissue, i.e., able to compensate such contribution. In this sense, the transmission line model proved itself as a practical tool also to analyze the impedance of a metasurface by simulating an impinging plane wave upon the structure depicted in Fig. 1(c). From the retrieved reflection coefficient and by supposing the air gap and the biological sample as known variables, the metasurface impedance $Z_{\text{meta}}$ can be extracted. Indeed, in this configuration, the new $Z_{\text{input}}$ can be evaluated as

$$Z_{input} = \frac{Z_0(1+\Gamma)}{(1-\Gamma)}. \tag{3}$$

It should be pointed out $Z_{\text{input}}$ is now given by the parallel between $Z_{\text{meta}}$ and $Z_1$ [which is supposed known, evaluated as in (1)].

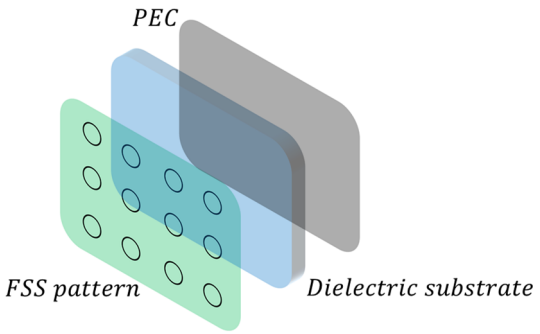


Fig. 2. Schematic draw depicting the structure of a typical AMC: a frequency-selective pattern is layered upon a PEC-backed dielectric substrate.

Clearly, it must be considered that human tissues can have a certain variability between different subjects and due to their inhomogeneous structure. Therefore, it is not possible to perfectly match a specific sample in a practical scenario; nonetheless, the overall impedance behavior remains the same (capacitive or inductive), making the designed metasurface an useful tool for matching purposes. Moreover, by adjusting the position of the metasurface in the space available between the antenna and the tissue, i.e., by adjusting the free space thickness $d_{\text{air}}$, it is possible to tune the metasurface impedance contribute according to the specific tissue.

### B. AMC for Radiating Performance Improvement

An AMC is a particular metasurface, whose typical structure includes a bidimensional array of resonating unit cells backed by a metallic ground (see Fig. 2).

As they appeared [42], [43], they have been first used as tools to improve the radiating performance of low-profile antennas. Indeed, they present a zero-crossing point in their phase response, from $\pi$ to $-\pi$, in correspondence to the unit-cells resonant frequency. This peculiar behavior is responsible of a reflected wave, which results in phase with the impinging wave (reflection coefficient equal to 1, instead of $-1$ of a PEC sheet). Therefore, the reflected wave creates a constructive interference without the need to leave any space between the antenna and the slab, as the traditional $\lambda/4$ gap in the presence of a PEC sheet. Thus, the overall radiating configuration is extremely compact, but, at the same time, the antenna gain can be increased, as well as the back radiation can be significantly reduced.

## III. Numerical Test-Case and Results

In this section, the adopted numerical test-case is presented. In particular, all the modeling and full-wave simulations have been performed through CST Microwave Studio Suite (Dassault Systèmes, France).

The radiating system is constituted by a classical bow-tie antenna [9], [44] operating at 2.56 GHz and in the close proximity of a biological phantom. As reported in Fig. 3(a), the proposed bow-tie is etched on the two faces of a 0.8 mm thick FR4 dielectric substrate ($\varepsilon_r = 4.3$ and $\tan\delta = 0.02$) by using a 35 $\mu$m thick copper strip line. The isosceles triangle

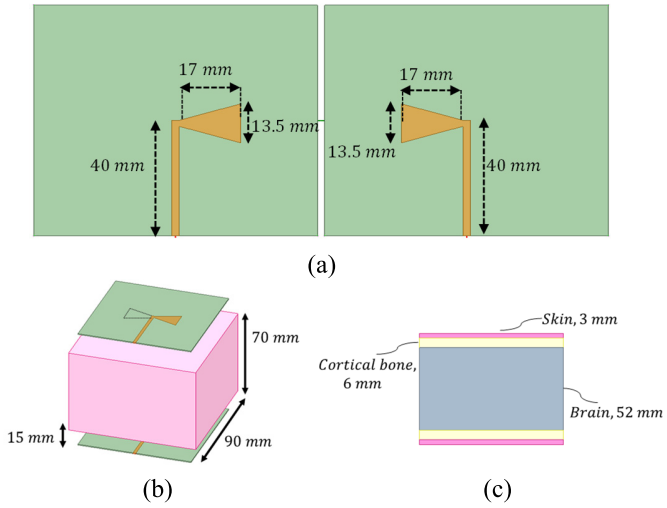


Fig. 3. (a) CAD representation of the designed bow-tie antenna: front (left) and bottom view (right). (b) CAD representation of the complete setup: two identical bow-tie antennas are separated by a biological phantom having the brain average dielectric properties. (c) Schematic of the phantom stratified model: a 3 mm thick skin layer together with a 6 mm thick bone layer is present above a brain tissue portion of 52 mm thickness.

height and base are 17 and 13.5 mm, respectively; conversely, the 50 Ω feeding strip line is 40 mm long and 2 mm wide. We adopted this antenna typology since it is representative for a high number of practical applications, but other antennas could have been chosen as well; the design guidelines and results can be easily generalized.

In order to evaluate the antenna behavior in the presence of a biological load, we created two simple but representative phantoms. Although biological tissues present a significantly dispersive behavior in terms of dielectric permittivity and electrical conductivity, nonetheless, we adopted a constant value for both these physical quantities for simplicity. Indeed, the radiating system under investigation is planned to work at a single frequency around 2.5 GHz. Therefore, by selecting a fixed value for the dielectric tissues properties (i.e., evaluated at 2.5 GHz), no significant errors are made. In detail, the first phantom consists in a cuboid of $90 \times 90 \times 70$ mm$^3$, with the average dielectric properties of the brain tissue ($\varepsilon_r = 43$ and $\tan\delta = 0.27$ at 2.5 GHz). The cuboid was placed 15 mm away from the bow-tie antenna. The complete setup, including two identical bow-ties separated by the biological load, is reported in Fig. 3(b); this configuration allows to evaluate the electromagnetic field transmission level within the tissue.

In addition, a more realistic phantom is designed, presenting the same overall dimensions and positioning with respect to the bow-tie antennas of the previous one. In this latter case, a stratified model is assumed: an external 3 mm thick skin layer ($\varepsilon_r = 42$ and $\tan\delta = 0.27$ at 2.5 GHz) together with a 6 mm thick cortical bone layer ($\varepsilon_r = 11.3$ and $\tan\delta = 0.25$ at 2.5 GHz) has been realized above the brain region, whose thickness is 52 mm [Fig. 3(c)].

At this point, we performed full-wave simulations to evaluate the two antennas behavior with and without the

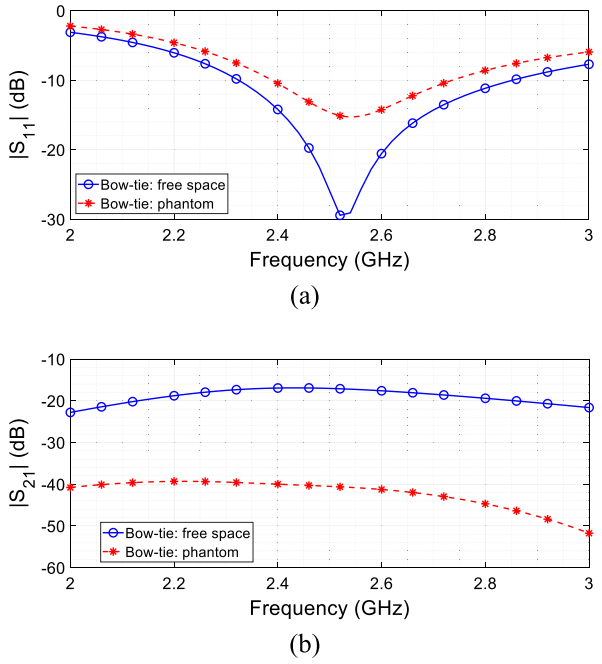


Fig. 4. S-parameters comparison between the two identical bow-tie antennas with (dashed line) and without (solid line) the homogeneous biological phantom, obtained through full-wave simulation. As evident from both the $S_{11}$ (a) and $S_{21}$ (b) parameters, the presence of biological phantom degrades the antenna performance.

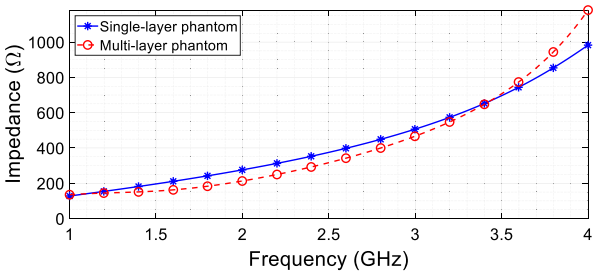


Fig. 5. Impedance behavior of the homogeneous (blue solid line) and stratified (red dashed line) biological phantoms considering an air gap of 15 mm according to the transmission line model. As evident, the homogeneous and stratified phantoms are similar, presenting an inductive behavior in the desired band.

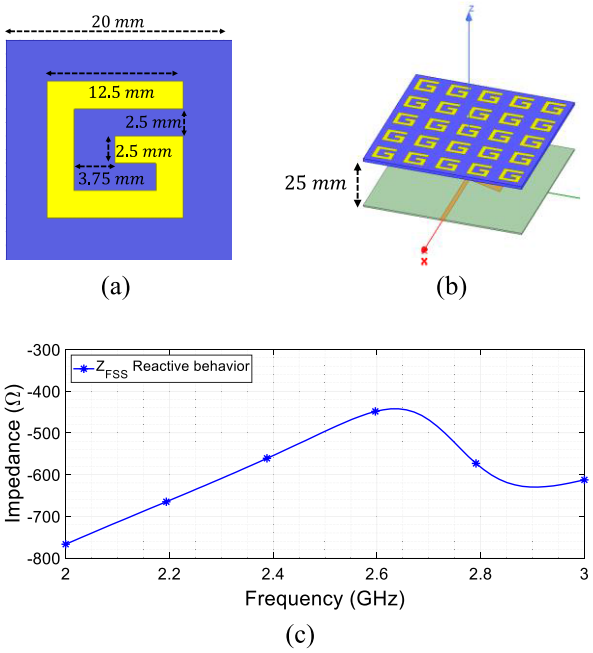


Fig. 6. CAD representation of the metasurface designed for impedance matching purposes. (a) Unit-cell geometrical details. (b) 5 × 5 array placed 25 mm above the bow-tie antenna. (c) Reactive behavior of the metasurface extracted following the transmission line model: the capacitive behavior is able to significantly counteract the inductive behavior of the tissue.

homogeneous biological phantom. The effect of the phantom in terms of detuning and mismatching can be evaluated from the $S_{11}$ parameter. On the other hand, the $S_{21}$ parameter is a measure of the field penetration inside the biological sample; in several applications, as, for instance, in imaging, the transmitted signal from one antenna to another is used to recreate the image. Therefore, it is an important parameter to be maximized in order to enhance the signal-to-noise ratio of the reconstructed image. As expected, the presence of phantom significantly degrades the performance of the antenna at the desired working frequency of 2.56 GHz (see Fig. 4).

For these reasons, we introduce in this section the design of metasurfaces for the impedance matching and the radiating performance enhancement.

### *A. Metasurfaces for Impedance Matching*

By following the design guidelines previously reported in Section II, the metasurface to be interposed between the antenna and the biological load to mitigate the impedance mismatch must be realized with an appropriate behavior (i.e., inductive or capacitive). Therefore, the preliminary step is to understand the tissue impedance nature at the desired frequencies, in order to guide the metasurface design. By using the transmission line model described in Fig. 1(b) and considering an air gap equal to 15 mm [see Fig. 3(b)], we extracted the simplified impedance of the equivalent circuit for both the homogeneous and the stratified phantom. As evident from Fig. 5, the biological load for the chosen test-case has an inductive behavior in the desired frequency band. This means that the metasurface should have an almost equal impedance contribute but opposite in sign (i.e., capacitive). Moreover, it can be appreciated that the homogeneous and the stratified phantom behave similarly within this frequency range; therefore, the simplified model can be properly employed for the general design of the system since the introduced approximation error is very limited.

In order to prevent the mismatch issue, we conceived a metasurface based upon the geometrical shape reported in Fig. 6(a), which is the result of an optimization procedure. The unit cell is etched with a 35 $\mu$m thick copper strip line over a 1.6 mm thick FR4 substrate ($\varepsilon_r = 4.3$ and $\tan\delta = 0.02$). The cell periodicity is 20 mm, whereas the remaining geometrical details are reported in Fig. 6(a). The metasurface is considered placed 15 mm away from the biological load, i.e., maintaining the previous air gap of the setup in Fig. 3(b). We performed the impedance extraction of this metasurface by relying on the simplified transmission line model [see (1)–(3)], and we obtained the result reported in Fig. 6(c). From this graph, it is apparent that the metasurface has a capacitive behavior within

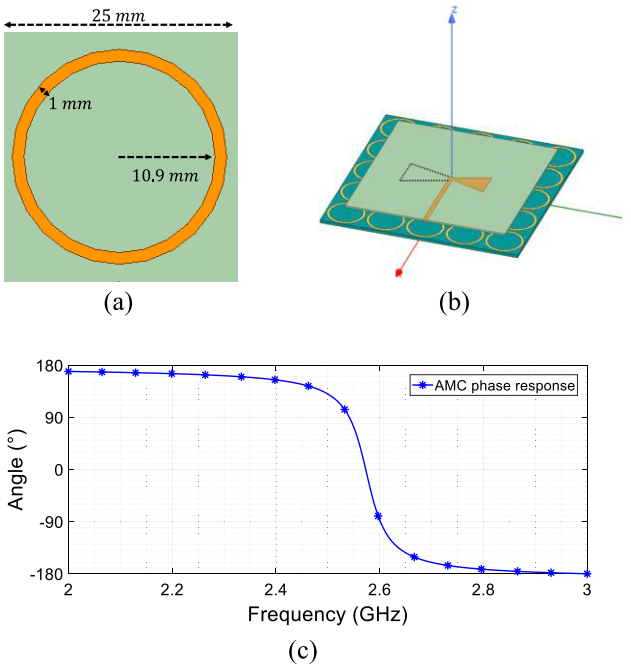


Fig. 7. CAD representation of the AMC designed for enhancing the bow-tie radiating performance. (a) Unit-cell geometrical details. (b) 5 × 5 array placed 3.5 mm below the bow-tie antenna. (c) Phase response of the proposed AMC when excited with a plane wave: the zero-cross point can be spotted at the desired frequency of 2.56 GHz.

the desired band and, in particular, a value close to the tissue impedance (but opposite in sign) around 2.56 GHz. Therefore, the designed metasurface is able to counteract the inductive behavior of the biological phantom.

Clearly, in order to be practically positioned within the proposed test-case, we realized a truncated version of the surface to be placed between the bow-tie and the phantom. Fig. 6(b) shows the 5 × 5 array placed 25 mm away from the bow-tie. It should be noticed that the exact positioning—the distance from the bow-tie—can be finely chosen to realize the desired tuning, as we described in Section II. This parameter can be used to change the metasurface impedance contribute and to match it to the specific tissue under consideration. Such empirical procedure provides an additional degree of freedom for the designer.

### B. AMC for Performance Increase

As introduced before, we also planned to insert an AMC as the backing element of the proposed bow-tie. Indeed, AMCs are structures able to improve the antenna performance, both in terms of higher gain and undesired back-radiation reduction. In several applications, such as, for instance, microwave imaging, it is important to achieve a significant field penetration inside tissues and the back radiation should be mitigated, both for interference reduction and users' safety. Therefore, we designed an appropriate AMC, by starting from the unit cell shown in Fig. 7(a). In particular, the loop is etched onto a 1.6 mm thick FR4 dielectric substrate with a 1 mm wide copper strip. The inner diameter was selected as 21.8 mm, whereas the overall cell periodicity was 25 mm; these geometrical parameters have been chosen to obtain the desired

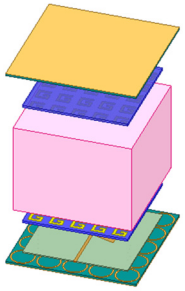

Fig. 8. CAD representation of the final radiating arrangement: a backing AMC, the bow-tie antenna, and the metasurface. In particular, the metasurface is positioned 15 mm away from the biological tissue as in the configuration of Fig. 3(b), thus ensuring a fair comparison between the two configurations.

response within the band of interest. By performing full-wave simulation through periodic boundary condition and a plane wave excitation, we extracted the frequency response of the proposed AMC. Fig. 7(c) reports the phase of the corresponding reflection coefficient, showing the typical AMC behavior where the phase passes from $\pi$ to $-\pi$. By observing this graph, the zero-cross point—where the reflection coefficient is equal to $+1$—can be highlighted around 2.56 GHz, as desired. For the front metasurface, we realized a truncated version of the AMC, in order to place the slab inside our setup. As Fig. 7(b) shows, a 5 × 5 array was positioned 3.5 mm below the bow-tie antenna, with the aim of enhancing the radiating behavior toward the positive values of $z$-axis and eliminating the undesired back-radiation.

### C. Complete Setup: AMC, Bow-Tie, and Metasurface

After the separate designs of the metasurface for impedance matching and the AMC for radiating performance enhancement, we finally assembled all the structures into a single system. In particular, Fig. 8 depicts the final arrangement; two identical radiating systems constituted by the backing AMC, the bow-tie antenna, and the metasurface are separated by the biological phantom already described in Fig. 3(b). By referring to Fig. 3(b), it is important to notice that the metasurface in the final setup was placed 15 mm away from the phantom; thus, the overall distance between the radiating system and the biological load has been maintained constant between the setup of Figs. 3(b) and 8. This ensures a fair comparison in terms of performance between the two configurations. Besides that, as previously described, the bow-tie antenna is placed 25 mm below the metasurface and 3.5 mm above the AMC.

After the final setup was assembled, we performed full-wave simulations to evaluate the related performance. Fig. 9 reports the S-parameters comparison between the two configurations (i.e., standalone bow-tie antennas against the case with AMC and metasurface), in the presence of the biological phantom. As evident from Fig. 9(a), both the configurations ensure a satisfactorily matching level, below the $-10$ dB threshold at the desired working frequency of 2.56 GHz.

Conversely, the adoption of the AMC and metasurface leads to a significantly enhancement of $S_{21}$, which is a direct measurement of the electromagnetic field transmission

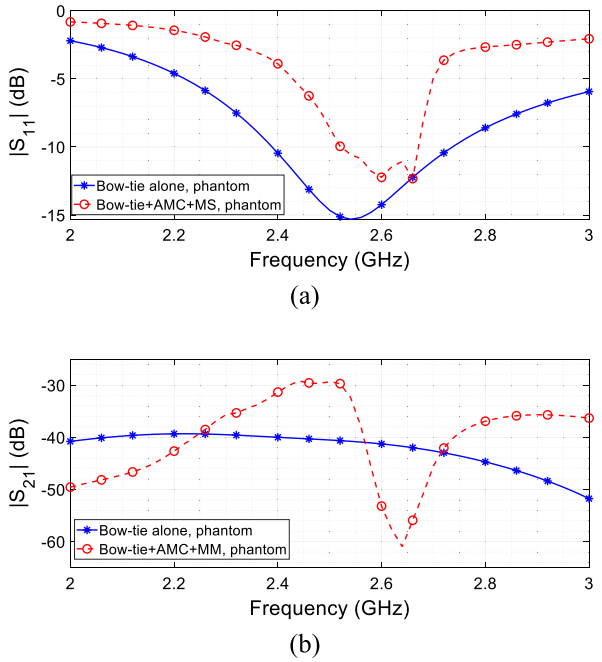


Fig. 9. Numerical S-parameters comparison between the setup constituted by two standalone bow-tie antennas (full line, blue) and the complete system including the AMC and the metasurface (dashed line, red), in both the cases in the presence of the biological phantom. (a) $S_{11}$. (b) $S_{21}$. As evident, the introduction of the AMC and the metasurface is able to preserve an acceptable matching level but significantly increase the wave transmission.

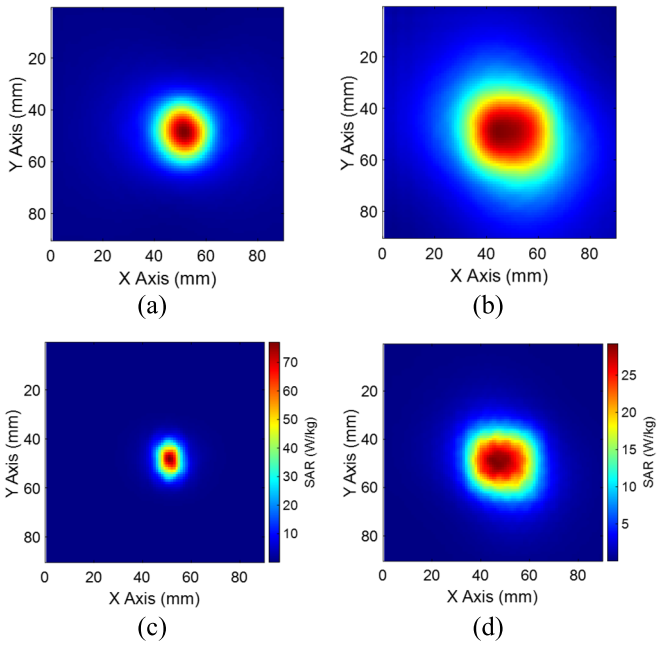


Fig. 10. (a) and (b) Normalized electric field map evaluated on the plane $xy$ in the middle of the biological homogeneous phantom: (b) AMC and metasurface configuration produces a field distribution more homogenous than (a) single bow-tie. SAR maps evaluated for an input power of 1 W for the case (c) without and (d) with AMC and metasurface, in a plane immediately inside the adopted phantom; as evident, the complete system is able to drastically reduce the SAR exposure for biological tissues in terms of SAR peak value.

within the biological phantom. Indeed, at the working frequency, we observed a +10.9 dB enhancement (from −40.6 to −29.7 dB), demonstrating the effectiveness of the proposed solution in mitigating the impedance mismatch in the presence of the tissue. This aspect can have a particularly significant and beneficial impact on imaging applications, as microwave imaging, where a higher level of transmission is strongly desirable to increase the signal-to-noise ratio as much as possible.

Another aspect to be carefully considered is relevant to the field distribution within the biological phantom. Indeed, for several applications, it is not sufficient that a higher transmission level is achieved, but also that the field distribution must be appropriate. Fig. 10(a) and (b) clearly shows that the AMC-metasurface configuration is able to produce a more homogeneous electric field distribution within the biological tissue. In particular, the normalized maps are evaluated on the $xy$ plane, in the middle of the phantom (see Fig. 8 for reference).

Strictly related to the electric field distribution, the specific absorption rate (SAR) is a fundamental parameter to be evaluated if the radiating system is envisioned to operate closely with human tissues. Therefore, we also performed full-wave simulations by feeding the stand-alone bow-tie antenna and the bow-tie in the presence of the two metasurfaces with the same input power (1 W, continuous wave). The SAR was evaluated immediately inside the biological phantom, since the electric field intensity is maximum closer to the radiating system (i.e., it represents the worst case). As evident from Fig. 10(c) and (d), the complete setup is able to drastically

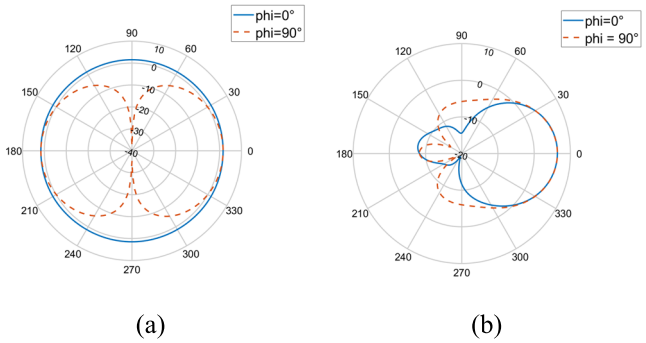


Fig. 11. (a) and (b) Bow-tie radiation patterns on two different planes ($\phi = 0°$ and $\phi = 90°$) for the case (a) without and (b) with AMC and metasurface. As evident, the AMC produces a higher gain and almost eliminates the back-radiation.

lower the SAR peak value, from 77.1 to 29.2 W/kg, spreading the absorbed energy on a larger area. This means that the proposed system is, in absolute, safer with respect to the stand-alone bow-tie antenna. It must be noticed that the evaluated SAR values exceed the limits expressed by the International Commission on Non-Ionizing Radiation Protection (ICNIRP) norms (2 W/kg) in both the configurations [45]. Therefore, the total admissible input power can be correspondingly scaled by the ratio of the obtained SAR values for the maximum allowed SAR.

Finally, Fig. 11(a) and (b) depicts the bow-tie antenna radiation patterns, on two different geometrical planes ($\phi = 0°$ and $\phi = 90°$). The radiation patterns, although are far-field characteristic features, are useful to verify the expected AMC behavior. In particular, the AMC-equipped bow-tie [see Fig. 11(b)]

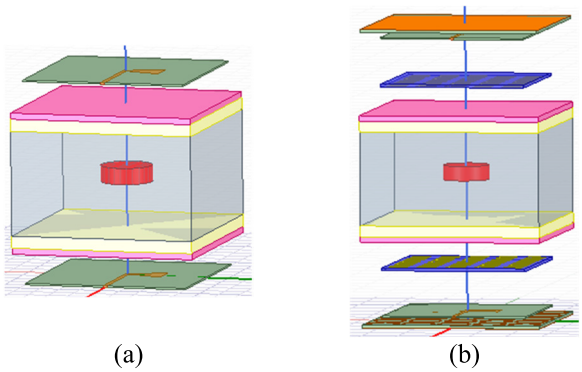

(a) (b)

Fig. 12. CAD models for the dielectric inclusion detection comparison between (a) stand-alone bow-tie and (b) complete system. As a more realistic scenario, we employed the stratified phantom with a blood inclusion placed in the middle of the brain region.

presents a higher gain and far less back-radiation than the standalone configuration [see Fig. 11(a)]. In many practical applications dealing with on-body antennas, it is desirable that the field penetrates into the tissues, but no field is required on the other half-space. In this sense, the backing AMC is able to accomplish both the results (higher gain and less back-radiation), proving itself as an effective antenna backing structure.

### D. Complete Setup: Dielectric Inclusion Detection

We demonstrated in the previous section that the proposed arrangement, i.e., including AMC and metasurface, is able to enhance the radiating performance of an antenna placed in the close proximity of a human body, both in terms of electric field penetration and higher antenna gain. Nevertheless, especially for imaging systems, it is fundamental to explore if this solution can also add some advantages with respect to the simple bow-tie in correctly spotting a dielectric inclusion present inside the tissue. Therefore, we first included within the stratified phantom reported in Fig. 3(c) an inclusion simulating a blood clot ($\varepsilon_r = 58.2$ and $\tan\delta = 0.32$ at 2.5 GHz). We adopted this phantom in order to simulate a more realistic and accurate scenario for this specific study. In particular, the cylindrical clot has been realized with a diameter of 25 mm and a height of 8 mm, positioned in the middle of the brain region (see Fig. 12).

At this point, we evaluated the difference between the $S_{21}$ parameter evaluated for the stratified phantom with and without the blood clot inclusion, respectively [12]. This quantity was calculated for both the radiating configurations, i.e., the stand-alone bow-tie antenna and the complete system including the AMC and the metasurface. The results from full-wave simulations have been reported in Fig. 13.

From the graph in Fig. 13, it is possible to conclude that the arrangement composed by the AMC and the metasurface is able to significantly increase the capability to detect a dielectric inclusion within the biological phantom. Indeed, the difference of the $S_{21}$ parameter passes from $-85$ dB for the stand-alone bow-tie to $-45$ dB for the complete system. Therefore, these results validated the overall design approach.

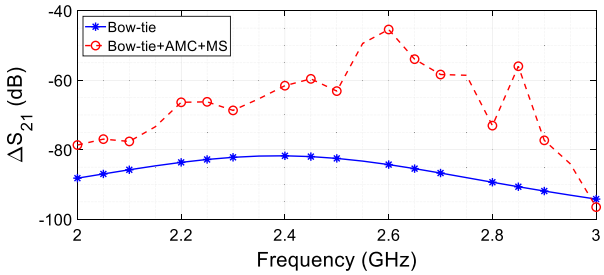


Fig. 13. $S_{21}$ parameter difference between the stratified phantom with and without the presence of the blood clot inclusion for the stand-alone bow-tie antenna (blue solid line) and the complete system including the AMC and the metasurface (red dashed line). As apparent, the proposed system is able to drastically enhance the capability to detect a dielectric inclusion within the biological volume.

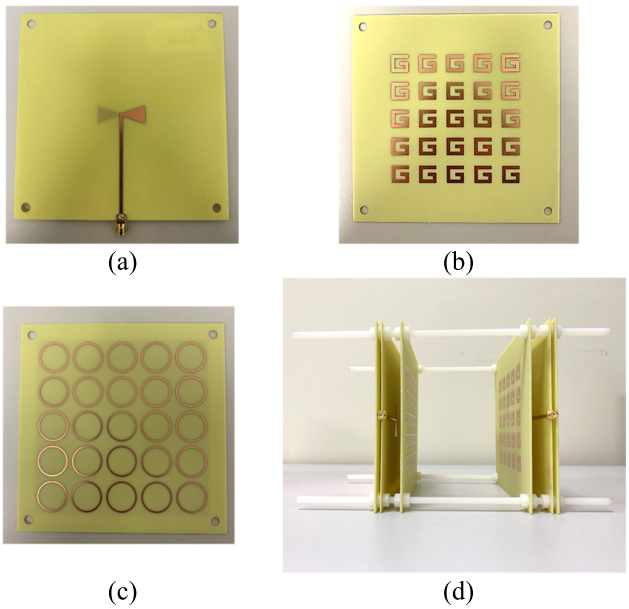

(a) (b) (c) (d)

Fig. 14. Fabricated prototypes by adopting PCB technology: all the system elements were realized with FR4 dielectric substrate. (a) Bow-tie front side. (b) Impedance matching metasurface. (c) AMC front side. (d) Complete radiating system with its positioning framework.

## IV. Prototype Fabrication and Measurements

In this section, we present the experimental measurements obtained over fabricated prototypes with the aim of validating the design methodology and the numerical simulations.

The various components of the radiating system were realized by adopting PCB technology. In particular, the chosen dielectric substrate was the epoxy resin FR4 ($\varepsilon_r = 4.3$ and $\tan\delta = 0.02$), as planned in the numerical design. The substrate and etched copper thicknesses and the geometrical details were also identical to the design section (see Fig. 14). The two bow-tie antennas were equipped with SMA connectors to allow the connection with the VNA (model N9918A, FieldFox Series, Keysight, Santa Rosa, CA, USA). In particular, as Fig. 14(d) shows, the PCB boards were also equipped with four external holes in order to create a nylon framework allowing an accurate positioning of the elements in terms of relative distance.

To consider the presence of a biological load closely positioned to the radiating system, we also realized a cylindrical

Fig. 15. Realized biological phantom: a plastic bottle filled with a solution of water, agar, and NaCl used to simulate the brain tissue.

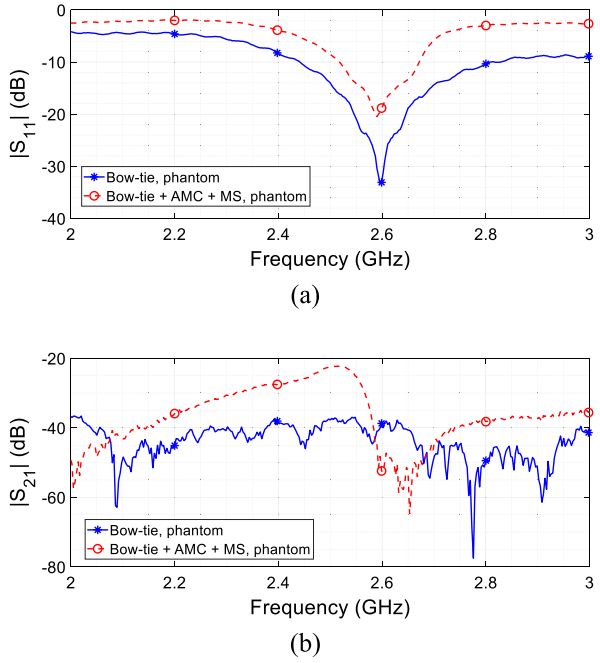


Fig. 16. Experimental S-parameters comparison between the setup constituted by two simple bow-tie antennas (full line, blue) and the complete system including the AMC and the metasurface (dashed line, red), in the presence of the biological phantom. (a) $S_{11}$. (b) $S_{21}$. The measurements confirmed the numerical results, where the matching level is preserved with the AMC and metasurface while the transmission level is significantly enhanced.

phantom (see Fig. 15). The container is 15 cm height, with a cross section of 9 cm and it was filled with a saline solution (NaCl 0.01 % w/v) made solid by adding agar at 3% w/v. In this way, the phantom similarly resembles in terms of dielectric properties the brain tissue adopted in the numerical simulations.

After the realized phantom was placed within the two radiating systems (transmitter and receiver), we acquired experimental measurements at the VNA. The measurements were performed for two different configurations: two standalone bow-tie antennas and two complete systems (AMC, bow-tie, and metasurface), separated by the biological phantom. Fig. 16 reports the S-parameters comparison between these two cases; the results confirmed the numerical simulations since the matching level was satisfactory for both the configurations, but the complete system with AMC and metasurface achieved

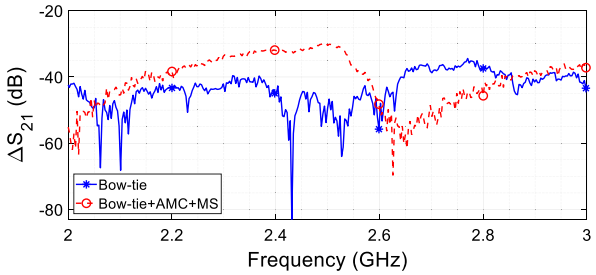


Fig. 17. Experimental $S_{21}$ parameter difference between the agar phantom with and without the presence of the dielectric inclusion for the stand-alone bow-tie antenna (blue solid line) and the complete system including the AMC and the metasurface (red dashed line). As evident, the proposed system is able to drastically enhance the capability to detect a dielectric inclusion within the biological volume.

a significantly higher coupling level, which passes from −37 to −22 dB, i.e., an increase of +15 dB.

After that, we also experimentally compared the performance of the complete system (AMC, metasurface, and bow-tie antenna) against the single bow-tie in detecting a dielectric target positioned inside the biological phantom. Therefore, we realized the inclusion, representing the blood clot, with the same size used in the numerical simulations (25 mm diameter and 8 mm height). The inclusion has been realized with a mixture of water, agar at 5% w/v, and NaCl at 2% w/v. The greater NaCl concentration has the role to simulate the higher conductivity of the blood with respect to the surrounding medium. In particular, we evaluated the difference between the $S_{21}$ parameter with and without the inclusion presence, for the two radiating configurations, as in the numerical simulations. The results, reported in Fig. 17, confirmed that the complete system composed by AMC, metasurface, and bow-tie antenna significantly outperforms the single bow-tie configuration in terms of dielectric target detection. Indeed, the $S_{21}$ difference between the presence and the absence of the inclusion roughly passed from around −45 to −30 dB at the operative frequency. As a matter of fact, the control over the dielectric properties of the experimental phantom cannot be precisely guaranteed as in simulations; nevertheless, the experimental results are in excellent agreement with the numerical ones.

To summarize, the performed numerical and experimental study demonstrated the possibility to integrate within the same radiating system an impedance matching metasurface and a backing AMC to increase the field penetration within the tissues and to enhance the overall radiating performance. To the best of our knowledge, this is the first attempt to combine similar structures in the same system, and the obtained results validates the design methodology.

## V. Conclusion

In this work, we presented a novel configuration for the radiating performance enhancement of antennas used for biomedical applications by adopting opportunely designed metasurfaces. In particular, we developed design guidelines, based on the transmission line model, to realize metasurfaces able to reduce the impedance mismatch caused by biological tissues closely placed to the radiating system. Furthermore,

we also introduce the simultaneous use of an AMC as the backing element of the system, exploiting its capability to reduce the potentially undesired back-radiation and to enhance the antenna gain. The combination of an impedance matching metasurface and of an AMC allows achieving a greater field penetration inside tissues and radiating performance enhancement.

To validate the design approach, we conceived a specific test-case, using a traditional bow-tie antenna closely positioned to a biological phantom. Both the numerical results and the experimental measurements obtained over fabricated prototypes demonstrated the validity of the proposed approach. These results can be extremely useful in several practical applications, where the radiating elements are close to the human body. Consumer applications can benefit from these compact solutions, but also industrial and medical fields can have positive impacts. For instance, microwave imaging and wireless power transfer systems for biomedical implants can be greatly optimized by adopting opportunely designed metasurfaces. Further developments will be directed to apply the obtained results on practical scenarios, optimizing the system design for the specific application.

## REFERENCES


[1] P. S. Hall and Y. Hao, *Antennas and Propagation for Body-Centric Wireless Communications*. Norwood, MA, USA: Artech House, 2012.

[2] M. Grimm and D. Manteuffel, "On-body antenna parameters," *IEEE Trans. Antennas Propag.*, vol. 63, no. 12, pp. 5812–5821, Dec. 2015, doi: 10.1109/TAP.2015.2482499.

[3] A. Yadav, V. K. Singh, A. K. Bhoi, G. Marques, B. Garcia-Zapirain, and I. de la Torre Díez, "Wireless body area networks: UWB wearable textile antenna for telemedicine and mobile health systems," *Micromachines*, vol. 11, no. 6, p. 558, May 2020, doi: 10.3390/mi11060558.

[4] M. Berg, T. Tuovinen, and E. T. Salonen, "Low-profile antenna with optimal polarization for 2.45 GHz on-body sensor nodes," in *Proc. Loughborough Antennas Propag. Conf. (LAPC)*, Nov. 2014, pp. 641–643.

[5] A. Lea, P. Hui, J. Ollikainen, and R. G. Vaughan, "Propagation between on-body antennas," *IEEE Trans. Antennas Propag.*, vol. 57, no. 11, pp. 3619–3627, Nov. 2009.

[6] F. Costa et al., "Wireless detection of water level by using spiral resonators operating in sub-GHz range," in *Proc. IEEE Int. Conf. RFID Technol. Appl. (RFID-TA)*, Sep. 2019, pp. 197–200, doi: 10.1109/RFID-TA.2019.8892141.

[7] S. Mondal, D. Kumar, S. Karuppuswami, and P. Chahal, "Scope and application of harmonic RFID for implanted body area network," in *Proc. IEEE Int. Conf. RFID (RFID)*, Sep. 2020, pp. 1–8.

[8] R. Chandra, H. Zhou, I. Balasingham, and R. M. Narayanan, "On the opportunities and challenges in microwave medical sensing and imaging," *IEEE Trans. Biomed. Eng.*, vol. 62, no. 7, pp. 1667–1682, Jul. 2015.

[9] X. Li, M. Jalilvand, Y. L. Sit, and T. Zwick, "A compact double-layer on-body matched Bowtie antenna for medical diagnosis," *IEEE Trans. Antennas Propag.*, vol. 62, no. 4, pp. 1808–1816, Apr. 2014.

[10] A. S. M. Alqadami, K. S. Bialkowski, A. T. Mobashsher, and A. M. Abbosh, "Wearable electromagnetic head imaging system using flexible wideband antenna array based on polymer technology for brain stroke diagnosis," *IEEE Trans. Biomed. Circuits Syst.*, vol. 13, no. 1, pp. 124–134, Feb. 2018.

[11] A. S. M. Alqadami, N. Nguyen-Trong, A. E. Stancombe, K. Bialkowski, and A. Abbosh, "Compact flexible wideband antenna for on-body electromagnetic medical diagnostic systems," *IEEE Trans. Antennas Propag.*, vol. 68, no. 12, pp. 8180–8185, Dec. 2020, doi: 10.1109/TAP.2020.2996815.

[12] E. Razzicchia, I. Sotiriou, H. Cano-Garcia, E. Kallos, G. Palikaras, and P. Kosmas, "Feasibility study of enhancing microwave brain imaging using metamaterials," *Sensors*, vol. 19, no. 24, p. 5472, Dec. 2019, doi: 10.3390/s19245472.

[13] D. Brizi et al., "Design of distributed spiral resonators for the decoupling of MRI double-tuned RF Coils," *IEEE Trans. Biomed. Eng.*, vol. 67, no. 10, pp. 2806–2816, Oct. 2020, doi: 10.1109/TBME.2020.2971843.

[14] S. Diana, D. Brizi, C. Ciampalini, G. Nenna, and A. Monorchio, "A compact double-ridged horn antenna for ultra-wide band microwave imaging," *IEEE Open J. Antennas Propag.*, vol. 2, pp. 738–745, 2021, doi: 10.1109/OJAP.2021.3089028.

[15] B. Sohani et al., "Detection of haemorrhagic stroke in simulation and realistic 3-D human head phantom using microwave imaging," *Biomed. Signal Process. Control*, vol. 61, Aug. 2020, Art. no. 102001.

[16] H. M. E. Misilmani, T. Naous, S. K. A. Khatib, and K. Y. Kabalan, "A survey on antenna designs for breast cancer detection using microwave imaging," *IEEE Access*, vol. 8, pp. 102570–102594, 2020, doi: 10.1109/ACCESS.2020.2999053.

[17] A. K. RamRakhyani and G. Lazzi, "Interference-free wireless power transfer system for biomedical implants using multi-coil approach," *Electron. Lett.*, vol. 50, no. 12, pp. 853–855, Jun. 2014, doi: 10.1049/el.2014.0567.

[18] A. Rajagopalan, A. K. RamRakhyani, D. Schurig, and G. Lazzi, "Improving power transfer efficiency of a short-range telemetry system using compact metamaterials," *IEEE Trans. Microw. Theory Techn.*, vol. 62, no. 4, pp. 947–955, Apr. 2014.

[19] D. Brizi, J. P. Stang, A. Monorchio, and G. Lazzi, "On the design of planar arrays of nonresonant coils for tunable wireless power transfer applications," *IEEE Trans. Microw. Theory Techn.*, vol. 68, no. 9, pp. 3814–3822, Sep. 2020, doi: 10.1109/TMTT.2020.2983145.

[20] M. Maldari, M. Albatat, J. Bergsland, Y. Haddab, C. Jabbour, and P. Desgreys, "Wide frequency characterization of intra-body communication for leadless pacemakers," *IEEE Trans. Biomed. Eng.*, vol. 67, no. 11, pp. 3223–3233, Nov. 2020, doi: 10.1109/TBME.2020.2980205.

[21] N. Nguyen, N. Ha-Van, and C. Seo, "Midfield wireless power transfer for deep-tissue biomedical implants," *IEEE Antennas Wireless Propag. Lett.*, vol. 19, no. 12, pp. 2270–2274, Dec. 2020, doi: 10.1109/LAWP.2020.3029848.

[22] A. Smida, A. Iqbal, A. J. Alazemi, M. I. Waly, R. Ghayoula, and S. Kim, "Wideband wearable antenna for biomedical telemetry applications," *IEEE Access*, vol. 8, pp. 15687–15694, 2020, doi: 10.1109/ACCESS.2020.2967413.

[23] A. Iqbal, M. Al-Hasan, I. B. Mabrouk, A. Basir, M. Nedil, and H. Yoo, "Biotelemetry and wireless powering of biomedical implants using a rectifier integrated self-diplexing implantable antenna," *IEEE Trans. Microw. Theory Techn.*, vol. 69, no. 7, pp. 3438–3451, Jul. 2021.

[24] C. J. Fox, P. M. Meaney, F. Shubitidze, L. Potwin, and K. D. Paulsen, "Characterization of an implicitly resistively-loaded monopole antenna in lossy liquid media," *Int. J. Antennas Propag.*, vol. 2008, pp. 1–9, Jan. 2008.

[25] P. M. Meaney, F. Shubitidze, M. W. Fanning, M. Kmiec, N. R. Epstein, and K. D. Paulsen, "Surface wave multipath signals in near-field microwave imaging," *Int. J. Biomed. Imag.*, vol. 2012, pp. 1–11, Jan. 2012.

[26] S. Maity, M. Nath, G. Bhattacharya, B. Chatterjee, and S. Sen, "On the safety of human body communication," *IEEE Trans. Biomed. Eng.*, vol. 67, no. 12, pp. 3392–3402, Dec. 2020, doi: 10.1109/TBME.2020.2986464.

[27] S. Genovesi, I. R. Butterworth, J. E. C. Serralles, and L. Daniel, "Metasurface matching layers for enhanced electric field penetration into the human body," *IEEE Access*, vol. 8, pp. 197745–197756, 2020, doi: 10.1109/ACCESS.2020.3034833.

[28] I. R. O. Connell, K. M. Gilbert, M. Abou-Khousa, and R. S. Menon, "Design of a parallel transmit head coil at 7T with magnetic wall distributed filters," *IEEE Trans. Med. Imag.*, vol. 34, no. 4, pp. 836–845, Apr. 2015, doi: 10.1109/TMI.2014.2370533.

[29] M. Alibakhshikenari et al., "A comprehensive survey on 'various decoupling mechanisms with focus on metamaterial and metasurface principles applicable to SAR and MIMO antenna systems,"' *IEEE Access*, vol. 8, pp. 192965–193004, 2020, doi: 10.1109/ACCESS.2020.3032826.

[30] M. Alibakhshikenari et al., "A comprehensive survey on antennas on-chip based on metamaterial, metasurface, and substrate integrated waveguide principles for millimeter-waves and terahertz integrated circuits and systems," *IEEE Access*, vol. 10, pp. 3668–3692, 2022, doi: 10.1109/ACCESS.2021.3140156.

[31] H.-T. Chen, J. Zhou, J. F. O'Hara, F. Chen, A. K. Azad, and A. J. Taylor, "Antireflection coating using metamaterials and identification of its mechanism," *Phys. Rev. Lett.*, vol. 105, no. 7, Aug. 2010, Art. no. 073901.

[32] M. Alibakhshikenari et al., "Metamaterial-inspired antenna array for application in microwave breast imaging systems for tumor detection," *IEEE Access*, vol. 8, pp. 174667–174678, 2020, doi: 10.1109/ACCESS.2020.3025672.
[33] J. B. Pendry, A. J. Holden, D. J. Robbins, and W. J. Stewart, "Magnetism from conductors and enhanced nonlinear phenomena," *IEEE Trans. Microw. Theory Techn.*, vol. 47, no. 11, pp. 2075–2084, Nov. 1999, doi: 10.1109/22.798002.
[34] H. An, G. Liu, Y. Li, J. Song, C. Zhang, and M. Liu, "Inhomogeneous electromagnetic metamaterial design method for improving efficiency and range of wireless power transfer," *IET Microw., Antennas Propag.*, vol. 13, no. 12, pp. 2110–2118, Oct. 2019.
[35] R. Pei et al., "Wearable EBG-backed belt antenna for smart on-body applications," *IEEE Trans. Ind. Informat.*, vol. 16, no. 11, pp. 7177–7189, Nov. 2020, doi: 10.1109/TII.2020.2983064.
[36] D. Brizi and A. Monorchio, "An analytical approach for the arbitrary control of magnetic metasurfaces frequency response," *IEEE Antennas Wireless Propag. Lett.*, vol. 20, no. 6, pp. 1003–1007, Jun. 2021, doi: 10.1109/LAWP.2021.3069571.
[37] M. A. Aldhaeebi, K. Alzoubi, T. S. Almoneef, S. M. Bamatraf, H. Attia, and O. M. Ramahi, "Review of microwaves techniques for breast cancer detection," *Sensors*, vol. 20, no. 8, p. 2390, Apr. 2020.
[38] M. Islam, M. Islam, M. Faruque, M. Samsuzzaman, N. Misran, and H. Arshad, "Microwave imaging sensor using compact metamaterial UWB antenna with a high correlation factor," *Materials*, vol. 8, no. 8, pp. 4631–4651, Jul. 2015, doi: 10.3390/ma8084631.
[39] M. Islam, M. Islam, M. Samsuzzaman, M. Faruque, N. Misran, and M. Mansor, "A miniaturized antenna with negative index metamaterial based on modified SRR and CLS unit cell for UWB microwave imaging applications," *Materials*, vol. 8, no. 2, pp. 392–407, Jan. 2015, doi: 10.3390/ma8020392.
[40] E. Razzicchia et al., "Metasurface-enhanced antennas for microwave brain imaging," *Diagnostics*, vol. 11, no. 3, p. 424, 2021.
[41] F. Costa, A. Monorchio, and G. Manara, "Efficient analysis of frequency-selective surfaces by a simple equivalent-circuit model," *IEEE Antennas Propag. Mag.*, vol. 54, no. 4, pp. 35–48, Sep. 2012, doi: 10.1109/MAP.2012.6309153.
[42] A. P. Feresidis, G. Goussetis, S. Wang, and J. C. Vardaxoglou, "Artificial magnetic conductor surfaces and their application to low-profile high-gain planar antennas," *IEEE Trans. Antennas Propag.*, vol. 53, no. 1, pp. 209–215, Jan. 2005, doi: 10.1109/TAP.2004.840528.
[43] D. J. Kern, D. H. Werner, A. Monorchio, L. Lanuzza, and M. J. Wilhelm, "The design synthesis of multiband artificial magnetic conductors using high impedance frequency selective surfaces," *IEEE Trans. Antennas Propag.*, vol. 53, no. 1, pp. 8–17, Jan. 2005.
[44] P. Takook, M. Persson, J. Gellermann, and H. D. Trefná, "Compact self-grounded Bow-Tie antenna design for an UWB phased-array hyperthermia applicator," *Int. J. Hyperthermia Thermal Therapies*, vol. 33, no. 4, pp. 387–400, 2017, doi: 10.1080/02656736.2016.1271911.
[45] A. Ahlbom et al., "Guidelines for limiting exposure to time-varying electric, magnetic, and electromagnetic fields (up to 300 GHz)," *Health Phys.*, vol. 74, no. 4, pp. 494–521, 1998.

**Danilo Brizi** (Member, IEEE) was born in Viterbo, Italy, in 1992. He received the M.S. Laurea degree (summa cum laude) in biomedical engineering and the Ph.D. degree (summa cum laude) in information engineering from the University of Pisa, Pisa, Italy, in 2016 and 2020, respectively.

From 2021, he is an Assistant Professor at the University of Pisa. His research interests include electromagnetic metasurfaces, MRI filter design, and wireless power transfer applications.

**Maria Conte** was born in Santeramo in Colle (BA), Italy, in 1993. She received the M.S. Laurea degree in biomedical engineering from the University of Pisa, Pisa, Italy, in 2021.

Since May 2021, she has been with Free Space SRL, Pisa, a company dealing with the design and industrialization of microwave and radio frequency systems.

**Agostino Monorchio** (Fellow, IEEE) is a Full Professor at the University of Pisa, Pisa, Italy. He has carried out a considerable research activity and technical consultancy to national, EU and U.S. industries, coordinating, as Principal Scientific Investigator, a large number of national and European research projects. He is the Director of RaSS National Laboratory, CNIT (Consorzio Nazionale Interuniversitario per le Telecomunicazioni), Parma, Italy. In 2012, he has been elevated to fellow grade by the IEEE for his contributions to computational electromagnetics and for the application of frequency selective surfaces in metamaterials. His research results have been published in more than 170 journal articles and book chapters and more than 260 communications at international and national conferences. He is the coauthor of four patents. He is active in a number of areas including computational electromagnetics, microwave metamaterials, radio propagation for wireless systems, the design and miniaturization of antennas and electromagnetic compatibility, and biomedical microwaves applications. The activity is mainly carried out at the Microwave and Radiation Laboratory (www.mrlab.it), Department of Information Engineering, University of Pisa, together with a large group of Ph.D. students, Post-Docotors, and Research Associates.

Prof. Monorchio has been an AdCom member from 2017 to 2019. He is a member of the Scientific Advisory Board of Directed Energy Research Center of TII, Abu Dhabi, United Arab Emirates, and affiliated with the Pisa Section of INFN, the National Institute of Nuclear Physics. He spent several research periods at the Electromagnetic Communication Laboratory, Pennsylvania State University, State College, PA, USA, both as a recipient of a scholarship (Fellowship Award) of the Summa Foundation, Albuquerque, NM, USA, and in the framework of CNR-NATO Senior Fellowship programme. He is the Co-Chair of the Industrial Initiative Committee of the IEEE APS. He serves as a Reviewer for international journals, and he was an Associate Editor of IEEE ANTENNAS AND WIRELESS PROPAGATION LETTERS from 2002 to 2007.

Open Access funding provided by 'Università di Pisa' within the CRUI CARE Agreement